Current Biology 22, 1616–1621, September 11, 2012 ©2012 Elsevier Ltd All rights reserved http://dx.doi.org/10.1016/j.cub.2012.06.055

Report

# *Drosophila* TRPML Is Required for TORC1 Activation

**Ching-On Wong,[1] Ruoxia Li,[3] Craig Montell,[3,*] and Kartik Venkatachalam[1,2,*]**
[1]Department of Integrative Biology and Pharmacology
[2]Graduate Programs in Cell and Regulatory Biology and Neuroscience, Graduate School of Biomedical Sciences University of Texas School of Medicine, Houston, TX 77030, USA
[3]Departments of Biological Chemistry and Neuroscience, Center for Sensory Biology, The Johns Hopkins University School of Medicine, Baltimore, MD 21205, USA

## Summary

**Loss-of-function mutations in TRPML1 (transient receptor potential mucolipin 1) cause the lysosomal storage disorder, mucolipidosis type IV (MLIV). Here, we report that flies lacking the TRPML1 homolog displayed incomplete autophagy and reduced viability during the pupal period—a phase when animals rely on autophagy for nutrients. We show that TRPML was required for fusion of amphisomes with lysosomes, and its absence led to accumulation of vesicles of significantly larger volume and higher luminal $Ca^{2+}$. We also found that *trpml*$^{1}$ mutant cells showed decreased TORC1 (target of rapamycin complex 1) signaling and a concomitant upregulation of autophagy induction. Both of these defects in the mutants were reversed by genetically activating TORC1 or by feeding the larvae a high-protein diet. The high-protein diet also reduced the pupal lethality and the increased volume of acidic vesicles. Conversely, further inhibition of TORC1 activity by rapamycin exacerbated the mutant phenotypes. Finally, TORC1 exerted reciprocal control on TRPML function. A high-protein diet caused cortical localization of TRPML, and this effect was blocked by rapamycin. Our findings delineate the interrelationship between the TRPML and TORC1 pathways and raise the intriguing possibility that a high-protein diet might reduce the severity of MLIV.**

## Results and Discussion

### Accumulation of Late Endosomes and Amphisomes in *trpml*$^{1}$

*Drosophila* transient receptor potential mucolipin (TRPML) localizes to late endosomes (LEs)/lysosomes in cultured cells [1]. To identify the subcellular localization of TRPML in vivo, we expressed a *UAS-trpml::myc* transgene in flies using the *GAL4/UAS* system [2]. TRPML::MYC decorated the periphery of LysoTracker-positive vesicles (Figures 1A–1C) and colocalized with the LE/lysosomal markers YFP::Rab7 (see Figures S1A–S1C available online) and lysosome-associated membrane protein:green fluorescent protein (LAMP::GFP) (Figures 1D–1F). These data indicate that TRPML::MYC is a LE/lysosomal membrane protein, as is the case for mammalian TRPML1 [3].

*Correspondence: cmontell@jhmi.edu (C.M.), kartik.venkatachalam@uth.tmc.edu (K.V.)

The *trpml*$^{1}$ flies are unable to complete lysosomal degradation of autophagosomes [1]. To identify the step in the lysosomal degradation pathway affected in *trpml*$^{1}$, we evaluated the degradation of the *Drosophila* Wnt homolog, Wingless (Wg) [4]. Following binding to its receptor, Wg is internalized into endosomes and degraded in lysosomes [5]. We found that there was increased accumulation of Wg in the wing pouch and notum of *trpml*$^{1}$ wing discs (Figures 1G, 1H, and 1K), and this phenotype was rescued by a *trpml*$^{+}$ genomic transgene (P[*trpml*$^{+}$];*trpml*$^{1}$) (Figure 1K).

Wg could be accumulating either in early endosomes or in LEs/multivesicular bodies (MVBs) in *trpml*$^{1}$ discs. To discriminate between these possibilities, we relied on the observation that Wg transmits signals at both the plasma membrane (PM) and early endosomes. Only after the formation of MVBs is the signal terminated. Therefore, increased Wg signaling in *trpml*$^{1}$ would suggest that Wg is accumulating in early endosomes, whereas unchanged Wg signaling would be consistent with Wg accumulating in MVBs. Therefore, we evaluated activation of the Wg target gene Hindsight (Hnt) in wing discs as described [4]. Nuclear Hnt expression was indistinguishable between wild-type (WT) and *trpml*$^{1}$ (Figures 1I and 1J), indicating that Wg signaling was not increased in *trpml*$^{1}$.

We also evaluated accumulation of Notch using an antibody specific for the endocytosed domain of Notch and found that levels of Notch increased dramatically in *trpml*$^{1}$ wing discs (Figures S1D and S1E; Figure 1K). Notch levels appeared higher than Wg in *trpml*$^{1}$ because whereas Wg accumulated in the wing pouch and notum, Notch was elevated over the whole disc. In support of the conclusion that the vesicles that accumulated in *trpml*$^{1}$ were LEs, the Notch-positive vesicles costained with LysoTracker (Figures S1F–S1H).

Autophagy is a pathway required for the degradation of cellular macromolecules that are too big to fit through the proteosomal barrel [6, 7]. During autophagy, double-membrane-bound vesicles called autophagosomes isolate the cytosolic material destined for degradation. Subsequently, autophagosomes fuse with LEs/MVBs to form amphisomes [8, 9]. Amphisomes then coalesce with lysosomes leading to the formation of autolysosomes. Because lysosomes carry degradatory enzymes, the contents of amphisomes are broken down following autolysosome formation [8, 9].

We previously reported that *trpml*$^{1}$ adults display hallmarks of decreased autophagic flux [1]. To provide evidence that there was accumulation of autophagosome and amphisomes, we stained WT and *trpml*$^{1}$ fat bodies with LysoTracker and GFP::ATG8. Autophagosomes are labeled with GFP::ATG8 only, whereas amphisomes are stained with both GFP::ATG8 and LysoTracker. Although WT showed virtually no GFP::ATG8 staining (Figure 1L), there were many *trpml*$^{1}$ vesicles that were labeled with GFP::ATG8 only or both GFP::ATG8 and LysoTracker (Figures 1M and 1N). These data indicated that loss of *trpml* led to an elevation of autophagosomes and amphisomes. Defects in receptor degradation have also been reported in human cells lacking TRPML1 and in *C. elegans* with a mutation disrupting the worm TRPML1 homolog [10–12]. These *trpml*$^{1}$ phenotypes closely resemble those of flies lacking *fab1* (vesicular phosphatidylinositol 3-phosphate

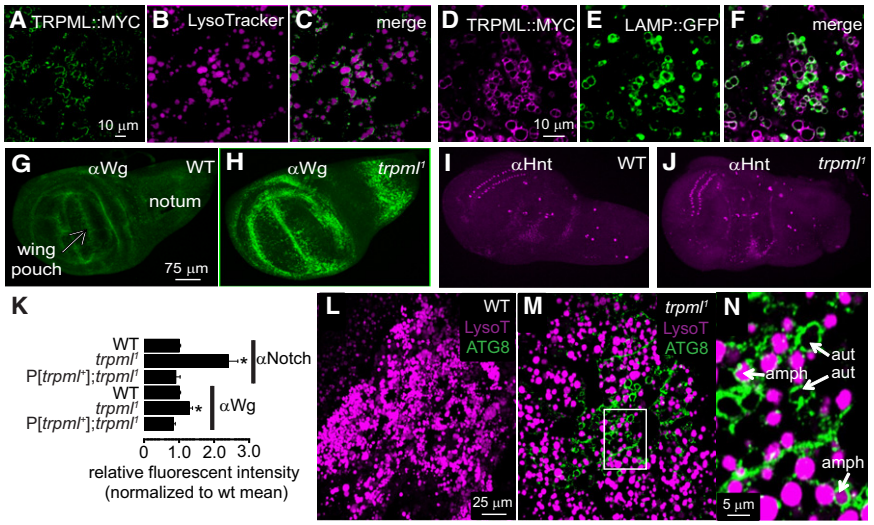


Figure 1. Increased Accumulation of LEs and Amphisomes in *trpml*$^{1}$ Mutants

(A–C) TRPML::MYC (A, green) decorates the periphery of LysoTracker-positive vesicles (B, magenta) in vivo. Confocal images of third-instar larval fat bodies dissected from animals expressing *UAS-trpml::myc* under the control of the fat body-specific *lsp2-GAL4*. The TRPML::MYC localization was detected using anti-MYC. (C) Merged image of (A) and (B). Scale bar shown in (A) applies to (A)–(C).

(D–F) TRPML::MYC (D, magenta) colocalizes with LAMP::GFP-positive vesicles (E, green) in vivo. Confocal images of third-instar larval fat bodies dissected from animals expressing *UAS-trpml::myc* under the control of the fat body-specific *cg-GAL4*. The TRPML::MYC localization was detected using anti-MYC. (F) Merged image of (D) and (E). Scale bar shown in (D) applies to (D)–(F).

(G–J) WT (G and I) and *trpml*$^{1}$ (H and J) third-instar larval (96 hr old) wing discs stained with (G and H) anti-Wg (αWg), (I and J) anti-Hnt (αHnt), and (N and O) anti-Notch (Notch). The scale bar shown in (G) applies to (G)–(J).

(K) Quantification of increased Wg and Notch fluorescent intensity in the *trpml*$^{1}$ and P[*trpml*$^{1}$];*trpml*$^{1}$ wing discs normalized to WT. Values represent mean ± SEM; *p < 0.05, Student's t test (n ≥ 3).

(L and M) Fat bodies dissected from normally fed WT (L) and *trpml*$^{1}$ (M) wandering third-instar larvae expressing *UAS-GFP::atg8* under the control of the fat-body driver *cg-GAL4*. The tissues were stained with anti-GFP (ATG8, green) and LysoTracker (LysoT, magenta). The scale bar shown in (L) also applies to (M).

(N) Magnified image of the boxed area from (M) showing autophagosomes (aut, vesicles labeled only by anti-GFP) and amphisomes (amph, vesicles labeled by both anti-GFP and LysoTracker).

See Figure S1.

5-kinase) [4]. These phenotypic similarities are consistent with the finding that the mammalian TRPML1 is activated by the product of Fab1/PIK-FYVE-kinase, PI(3,5)P(2) [13].

### Defects in the Fusion of Amphisomes with Lysosomes

We also performed electron microscopy (EM) on larval fat bodies to confirm the nature of the accumulating vesicles based on previously described morphological criteria [14]. WT fat-body cells contained large electron-dense, lysosome-like structures (Figures 2A and 2C). Many of these lysosomes were in the process of fusing and appeared as "figure 8"-like structures without internal separations (Figure 2A and blue lines in Figure 2C). In contrast, *trpml*$^{1}$ fat-body cells contained substantially fewer and smaller lysosomes (Figure 2B). This phenotype resembles that observed in *deep orange* (*dor*) mutant fat bodies, which are characterized by diminished fusion of LEs with lysosomes [14]. Furthermore, *trpml*$^{1}$ mutant cells accumulated large single-membrane-bound vesicles that contained smaller internal vesicles indicating that they were MVBs/amphisomes (Figures 2B, 2D, and 2E). Many of these vesicles were touching lysosomes, apparently unable to undergo fusion (Figures 2D and 2E). We propose that these "fusion-clamped" vesicles arise from a defect in fusion of MVBs and/or amphisomes with lysosomes in *trpml*$^{1}$. The *trpml*$^{1}$ fat bodies also showed fusion-clamped lysosomes (Figure 2F), indicating that both homotypic and heterotypic fusions of vesicles were disrupted.

To quantify the increased vesicle accumulation in *trpml*$^{1}$, we performed EM on adult photoreceptor cells (PCs), which are more amenable to quantification than the cells of the fat bodies because the cell boundaries are more clearly evident in the former. We found that whereas WT PCs showed very few MVBs (single-membrane-bound vesicles with internal vesicular structures) and lysosomes (electron-dense multilamellar structures) per section, *trpml*$^{1}$ PCs displayed a dramatic elevation of both MVBs and lysosomes (Figures S2A, S2B, and S2G). The mutant cells also showed increased accumulation of autophagosomes (double-membrane-bound vesicles containing cytosolic material) (Figure S2G). Higher levels of autophagosomes in adult PCs were consistent with the finding in larval fat bodies. The relative numbers of autolysosomes, which formed after fusion of MVBs and lysosomes (single-membrane-bound vesicles containing internal vesicular structures and multilamellar electron-dense lysosomes), were not significantly different in WT and *trpml*$^{1}$ cells despite an increase in amphisomes and lysosomes (Figure S2G). Furthermore, the ratio of MVBs:autolysosomes was 10-fold higher in *trpml*$^{1}$ compared to WT (11.7 and 1.2, respectively; Figure S2G). The *trpml*$^{1}$ PCs also contained many MVBs that were touching lysosomes (2.2 ± 0.8 fusion-clamped vesicles/ommatidia in *trpml*$^{1}$ mutants) (Figures S2C–S2G). The number of these "fusion-clamped" vesicles was significantly lower in WT cells (0.1 ± 0.1 fusion-clamped vesicles/ommatidia; p = 0.04, Student's t test) (Figure S2G). Taken together, our data point to a defect in the fusion of MVBs with lysosomes in *trpml*$^{1}$ cells. Furthermore, because the total number of autolysosomes is unchanged in the mutants, we suggest that they display an additional defect in lysosomal degradation.

### Elevated LE $Ca^{2+}$ in the *trpml*$^{1}$ Mutants

Mammalian TRPML1 is a LE/lysosomal channel responsible for the release of luminal $Ca^{2+}$ [13, 15, 16]. Therefore, loss of TRPML1 might lead to elevated LE $Ca^{2+}$ levels. To investigate whether elimination of *Drosophila trpml* led to elevated LE $Ca^{2+}$ levels, we measured the releasable pool of LE luminal $Ca^{2+}$ in fura-2-loaded fat bodies. For releasing LE $Ca^{2+}$ we treated the fat bodies with bafilomycin A1—a cell-permeant inhibitor of the vacuolar-type $H^{+}$-ATPase. Treatment with

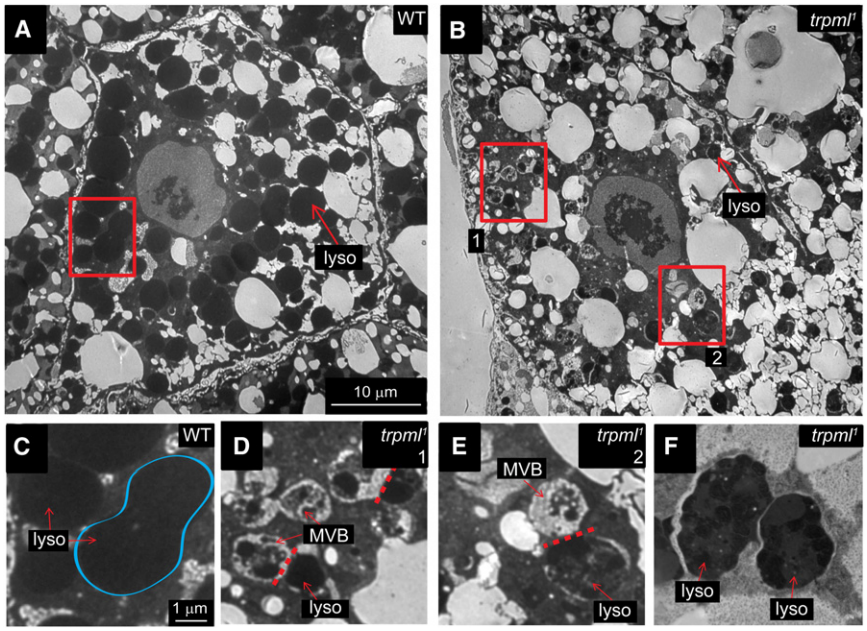


Figure 2. Ultrastructural Analyses of Vesicle Fusion Defects in *trpml*$^{1}$

(A and B) Representative transmission EM images of normally fed WT (A) and *trpml*$^{1}$ (B) wandering third-instar larval fat bodies. The scale bar shown in (A) also applies to (B).

(C) Magnified image of the boxed area shown in (A). Blue line indicates two lysosomes in the process of fusing. Scale bar shown in (C) also applies to (D)–(F).

(D) Box 1 from (B).

(E) Box 2 from (B).

(F) Magnified image showing two fusion-clamped lysosomes.

The structures labeled include lysosomes (lyso) and MVBs. The dashed red lines indicate the area of contact between the "fusion-clamped" vesicles.

See Figure S2.

bafilomycin A1 results in loss of the LE $H^+$ gradient and eventual depletion of LE $Ca^{2+}$, which increases the cytosolic-free $Ca^{2+}$ concentration [17]. Consistent with the notion that the *trpml*$^{1}$ mutants had elevated LE $Ca^{2+}$ levels, bafilomycin A1 treatment caused a significant elevation in cytosolic-free $Ca^{2+}$ in *trpml*$^{1}$ compared to WT (0.03 ± 0.006 and 0.15 ± 0.05 in WT and *trpml*$^{1}$, respectively) (Figure S3A; Figures 3A, and 3B). These data indicated that *trpml*$^{1}$ LEs contained higher levels of $Ca^{2+}$ due to diminished $Ca^{2+}$ release.

### Increased Induction of Autophagy Due to Decreased TORC1 Activity in *trpml*$^{1}$

We compared the sizes of LysoTracker-positive vesicles in WT and *trpml*$^{1}$ larval fat bodies to assess autophagy induction [18]. Consistent with increased induction of autophagy in *trpml*$^{1}$, there was a striking elevation in the volume of LysoTracker-positive vesicles in mutant fat bodies (Figures 3C, 3D, and 3F). This change became evident and was most pronounced in fat bodies from second-instar larvae (8.14- ± 1.7-fold larger in *trpml*$^{1}$) (Figure 3F). The difference between WT and *trpml*$^{1}$ was less pronounced but still significant in third-instar larvae (2.77- ± 0.5-fold increase in *trpml*$^{1}$) (Figure 3F). The smaller elevation in *trpml*$^{1}$ third-instar larvae likely reflects ecdysone-dependent autophagy activation in WT tissues at this developmental stage [14, 19].

We hypothesized that induction of autophagy without its completion should suppress target of rapamycin complex 1 (TORC1) activity due to two factors. First, a decline in autophagic flux would decrease net availability of amino acids that are produced via autophagic degradation of proteins [20]. Reduced amino acid levels would diminish activity of the TORC1 [21–23]. Indeed, diminished autophagic flux by Atg7 knockdown led to reduced TORC1 activity as determined by phosphorylation of the TORC1 substrate, S6 kinase (pS6K) [21, 24]. We found a similar decrease in TORC1 activity after knocking down Atg5 in WT fat bodies using RNAi (Figures S3B and S3C). Second, increased autophagy will directly suppress TORC1 function because autophagy and TORC1 activity are mutually antagonistic [24]. Decreased TORC1 will induce further induction of autophagy leading to the generation of larger LysoTracker-positive vesicles.

Several lines of evidence support the preceding proposal. First, feeding *trpml*$^{1}$ third-instar larvae protein-rich yeast paste suppressed the increase in the volume of LysoTracker-positive vesicles (Figures 3E and 3F). Second, pS6K was diminished in *trpml*$^{1}$ fat bodies (Figures 3G and 3H). The decrease in pS6K in *trpml*$^{1}$ was reversed by driving WT *trpml*$^{+}$ in fat bodies using *cg-GAL4* [25] (Figure 3H). Furthermore, yeast feeding suppressed the reduction in pS6K levels in *trpml*$^{1}$ (Figures 3G and 3H). To investigate whether decreased TORC1 activity occurs in other mutants with diminished fusion of LEs with lysosomes, we evaluated pS6K in *dor* mutants [14, 26]. Extracts from *dor*$^{4}$ mutant larvae showed a reduction in pS6K (Figure 3H). Therefore, a block in the fusion of LEs with lysosomes results in decreased cellular amino acid levels and decreased TORC1 activity.

Third, genetically upregulating TORC1 activity in mutant fat bodies by overexpressing Rheb and constitutively active Rag ($Rag^{Q61L}$) [27, 28] decreased the LysoTracker-positive vesicular volume (Figure S3D). Vesicular volume in *trpml*$^{1}$ did not increase any further when we expressed dominant-negative Rag ($Rag^{T16N}$) [27], indicating that Rag activity was already maximally reduced in *trpml*$^{1}$. The finding that elevating TORC1 activity is sufficient to suppress lysosomal storage argues that the increase in acidic vesicles in *trpml*$^{1}$ reflects a decrease in TORC1 activity. Therefore, elevating TORC1 activity is sufficient to prevent vesicle accumulation despite the persistence of vesicle fusion defects.

Finally, the half-maximal time to pupation was increased in *trpml*$^{1}$ (Figure S3E). Because decreased TORC1 activity causes a developmental delay [29], these data are also consistent with a decrease in TORC1 activity in *trpml*$^{1}$. Feeding the larvae protein-rich yeast paste restored pS6K levels to WT (Figures 3G and 3H) and rescued the defect in developmental timing (Figure S3E).

LE/lysosomal $Ca^{2+}$ is required for the homotypic and heterotypic fusion of these vesicles [30]. Therefore, the increased LysoTracker staining in *trpml*$^{1}$ may have resulted from diminished $Ca^{2+}$ release from the vesicles leading to impaired fusion of the LEs/amphisomes with lysosomes, ultimately resulting in reduced degradation of their contents.

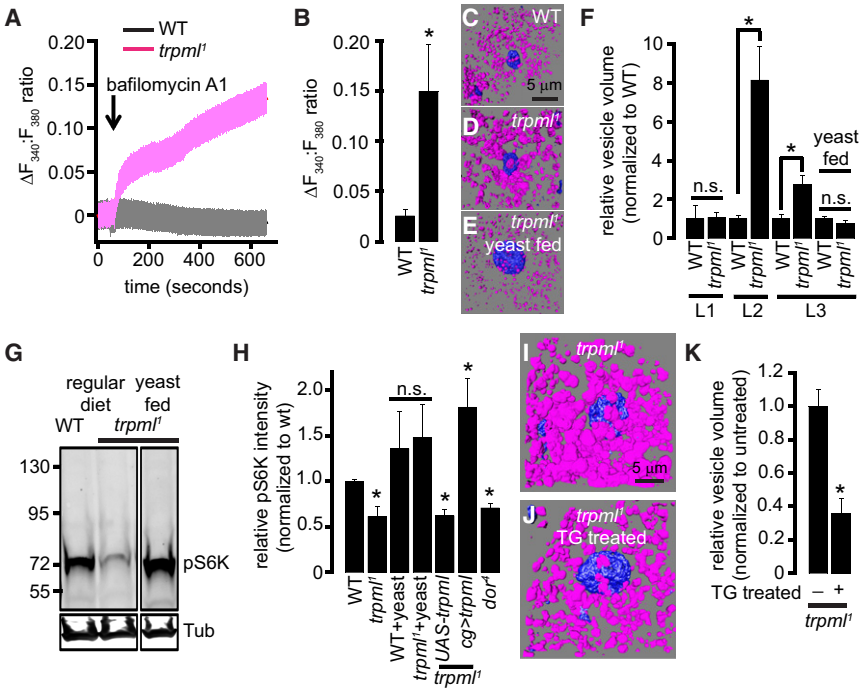


Figure 3. Elevated Lysosomal $Ca^{2+}$, Increased Induction of Autophagy, and Decreased TORC1 Signaling in the *trpml*$^{1}$ Mutants

(A) Graph showing overall changes in $F_{340}$:$F_{380}$ ratio in WT (black) and *trpml*$^{1}$ (magenta) tissues. Arrow represents point at which bafilomycin A1 was added. Values represent mean ± SEM (n = 70 cells of each genotype [seven separate experiments with approximately ten cells per experiment].

(B) Bar graph showing change in fura-2 $F_{340}$:$F_{380}$ ratio from t = 0 s to t = 600 s. Values represent mean ± SEM. *p < 0.05, Student's t test (n = 7 experiments per genotype).

(C–E) Volumetric three-dimensional reconstructions of a 400 $mm^2$ area (20 × 20 mm) showing LysoTracker (magenta) and DAPI (blue)-stained third-instar larval fat bodies of the indicated genotypes and feeding status. The scale bar shown in (C) is applicable to (C)–(E).

(F) Volumes of LysoTracker-positive vesicles in fat bodies dissected from first-, second-, and third-instar WT and *trpml*$^{1}$ larvae (L1–L3, respectively). Values were normalized to WT for each larval stage. Values represent mean ± SEM. *p < 0.05, Student's t test (n = 5–7 animals of each genotype). n.s., not significant.

(G) Representative western blot of larval fat-body extracts derived from WT and *trpml*$^{1}$ and yeast-fed *trpml*$^{1}$ third-instar larvae probed with antibodies against pS6K and α-tubulin (Tub).

(H) Quantification of relative pS6K intensities in fat-body extracts derived from wandering third-instar larvae of the indicated genotypes and feeding status. Values were normalized to WT. Values represent mean ± SEM. *p < 0.05, Student's t test (n = 5–9 independent western blots using different samples each time). The term *cg* refers to *cg-GAL4*, a fat body and hemocyte-specific driver.

(I and J) Volumetric three-dimensional reconstructions of a 400 $mm^2$ area (20 × 20 mm) showing LysoTracker (magenta) and DAPI (blue)-stained third-instar *trpml*$^{1}$ larval fat bodies. (J) shows LysoTracker-positive vesicles after thapsigargin (TG) treatment. The scale bar shown in (I) is applicable to (I) and (J).

(K) Bar graph showing the relative volumes of LysoTracker-positive vesicles in fat bodies dissected from third-instar *trpml*$^{1}$ larvae that were either untreated or treated with TG. Values were normalized to the untreated samples. Values represent mean ± SEM. *p < 0.05, Student's t test (n = 9 animals of each genotype).

See Figure S3.

Consistent with the proposal that increased vesicular volume stemmed from diminished $Ca^{2+}$ release, treatment of the fat bodies with thapsigargin, which blocks the sarcoplasmic/endoplasmic reticulum calcium ATPase pump and causes $Ca^{2+}$ release from endoplasmic reticulum stores, resulted in a significant decrease in the volume of LysoTracker-positive vesicles in *trpml*$^{1}$ (Figures 3I–3K). Therefore, despite the absence of a LE $Ca^{2+}$ release mechanism in *trpml*$^{1}$, elevation of cytosolic $Ca^{2+}$ levels from a different $Ca^{2+}$ reserve was sufficient to partially suppress the increase in LysoTracker-positive vesicle volume. Although our data are most consistent with a defect in the fusion of vesicles in *trpml*$^{1}$, we cannot rule out that there may also be a defect in vesicular trafficking, thereby reducing encounters between fusible vesicles.

### Suppression of *trpml* Semilethality by High-Protein Diet

During the pupal period *Drosophila* do not feed, and they depend on autophagy for the amino acids necessary for morphogenesis and survival. Loss of *trpml* causes semilethality during the pupal period because <10% of adults eclose from the pupal cases (Figure 4A; Figure S4C) [1]. To test whether this reduced viability resulted from an insufficient supply of amino acids, we fed the mutant larvae a high-protein diet (food supplemented with 20% w/v yeast). We found that this diet significantly suppressed the lethality (Figure 4A; Figure S4C). However, the effects of another mutation that caused pupal lethality (P element inserted in *vamp-7*, *CG1599*$^{EY09354}$; Figures S4A and S4B) were not suppressed by yeast supplementation (Figure S4C).

The suppression of the *trpml* semilethality by yeast paste could have been due to either protein or carbohydrates in this supplement. Therefore, we tested whether supplementation of either tryptone or sucrose diminished the lethality. We found that whereas tryptone supplementation reduced the semilethality, sucrose supplementation did not (Figure 4B; Figure S4D). The lack of suppression with sucrose indicated that the phenotype was not a result of caloric deprivation but rather reflected a requirement for increased dietary amino acids by *trpml*$^{1}$ larvae.

Next, we considered whether the suppression of the semilethality by the high-protein diet was due to increased TORC1 activity. We fed yeast paste to *trpml*$^{1}$ larvae in the presence of the TORC1 inhibitor, rapamycin. We found that rapamycin prevented suppression of the pupal semilethality by yeast paste (Figure S4E). Moreover, rapamycin enhanced the lethality when *trpml*$^{1}$ larvae were reared on normal food (Figure 4C). However, feeding the *dor* mutants rapamycin did not decrease their viability (data not shown). These data indicate that not all mutants with deficient fusion of LEs to lysosomes show increased sensitivity to rapamycin.

TORC1 simultaneously increases protein translation and decreases autophagy. One of the ways through which TORC1 increases protein translation is phosphorylation and inhibition of the translational suppressor Thor—fly homolog of 4E-BP1 [31, 32]. Therefore, if the effects of TORC1 activation

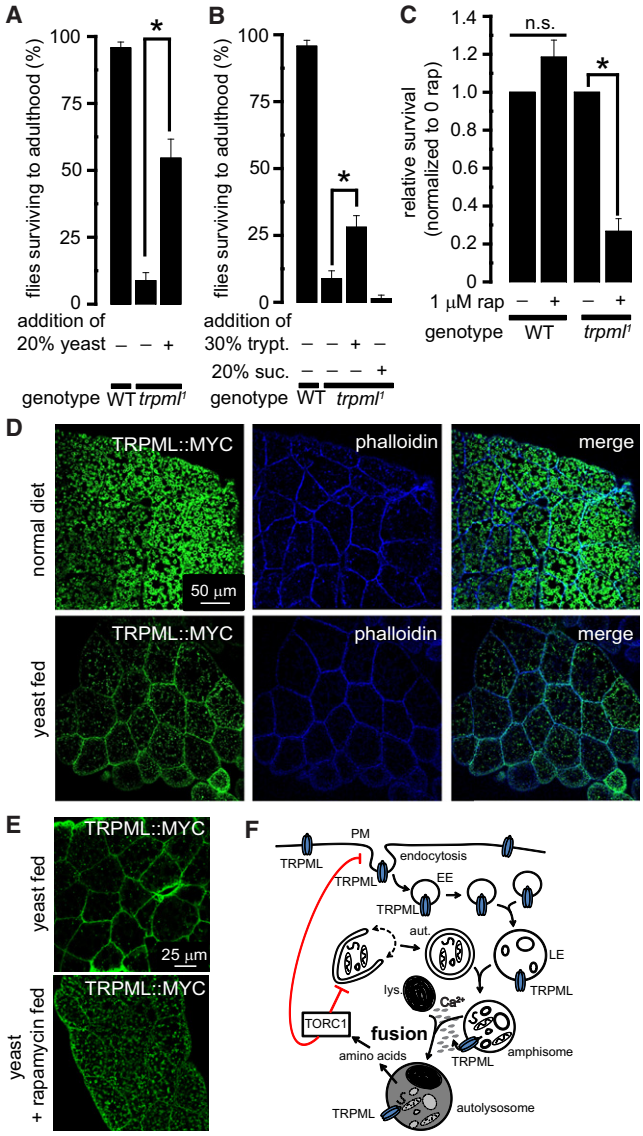


Figure 4. Activating TORC1 by Feeding Larvae a Protein-Rich Diet Suppresses the Toxicity Associated with the Loss of *trpml*$^{1}$

(A) Bar graph showing survival of flies of the indicated genotypes that were reared on either standard food or food containing 20% yeast. Values represent mean ± SEM. *p < 0.05, Student's t test (n ≥ 3 independent fly vials).

(B) Bar graph showing survival of flies of the indicated genotypes that were reared on either standard food or food containing the indicated additional feedants: trypt. (tryptone) or suc. (sucrose). Values represent mean ± SEM. *p < 0.05, ANOVA followed by pairwise Student's t test with Bonferroni post hoc corrections (n ≥ 3 independent fly vials).

(C) Relative survival of WT and *trpml*$^{1}$ animals through the pupal period when reared on food in the presence or absence of 1 μM rapamycin (rap). The values were normalized to the survival of flies reared without rapamycin. Values represent mean ± SEM. *p < 0.05, Student's t test; n.s., no significance (n ≥ 3 independent fly vials).

(D) Confocal images showing TRPML::MYC (green) and phalloidin (blue) staining in fat bodies dissected from third-instar larvae expressing *UAS-trpml::myc* under the control of the *cg-GAL4*. The tissues dissected from yeast-fed larvae are indicated. The scale bar shown in the top left panel is applicable to all of the panels.

(E) Confocal images showing TRPML::MYC staining in fat bodies dissected from third-instar larvae expressing *UAS-trpml::myc* under the control of *cg-GAL4*. The tissues dissected from yeast-fed and yeast + rapamycin-fed larvae are indicated. The scale bar shown in the left panel is applicable to both panels.

in *trpml*$^{1}$ depend upon protein translation, then rapamycin should not reverse the beneficial effect of yeast feeding in *thor*$^{2}$;*trpml*$^{1}$ double-mutant animals. However, yeast paste still suppressed the semilethality in *thor*$^{2}$;*trpml*$^{1}$ double mutants (no *thor*$^{2}$;*trpml*$^{1}$ adults eclosed in the absence of yeast-supplemented diet), and the effect of rapamycin remained unchanged (Figure S4E). These results suggest that activation of TORC1 by high levels of amino acids may have suppressed the pupal semilethality of *trpml*$^{1}$ by decreasing autophagy rather than by increasing protein translation.

## TORC1 Regulates the Subcellular Localization of TRPML

To investigate whether TORC1 activity reciprocally affected TRPML, we examined the spatial distribution of TRPML::MYC under conditions in which we manipulated TORC1 activity. On a normal diet, TRPML::MYC was exclusively intracellular (Figure 4D). However, on a high-protein diet, TRPML::MYC colocalized with the cortical F-actin marker phalloidin (Figure 4D), indicating that TRPML was at the PM. In larvae maintained on a high-protein diet and rapamycin, we detected TRPML::MYC exclusively in intracellular vesicles (Figure 4E). These data indicate that the PM localization of TRPML::MYC depends on the activity of TORC1. Further supporting this conclusion, TRPML::MYC was predominantly localized to the PM in larval salivary glands (Figure S4F), which are characterized by low levels of autophagy (and therefore high TORC1 activity) till the onset of the pupal phase, when autophagy is required for the degradation of the pupal salivary gland during metamorphosis [33].

The effect of TORC1 activity on the subcellular location of TRPML is unlikely to reflect alterations in bulk endocytosis because TORC1 enhances rather than suppresses bulk endocytosis [34, 35]. Rather, we suggest that by occluding entry of TRPML into endosomes and diminishing the levels of TRPML in the LEs, TORC1 exerts feedback regulation on the completion of autophagy. Therefore, in addition to suppressing the initiation of autophagy [24], TORC1 also inhibits the completion of autophagy by regulating the subcellular location of TRPML.

## Model of TRPML Function and Concluding Remarks

TRPML is a $Ca^{2+}$ channel, which is endocytosed from the PM and eventually enters the LEs (Figure 4F). The LEs fuse with autophagosomes creating amphisomes. TRPML present in amphisomes releases luminal $Ca^{2+}$ to facilitate $Ca^{2+}$-dependent fusion of amphisomes with lysosomes. The amino acids generated by degradation of proteins in the autolysosomes promote TORC1 activation. In addition to inhibiting the initiation of autophagy, activated TORC1 also diminishes endocytosis of TRPML.

In the absence of TRPML, fusion of amphisomes and lysosomes is impaired. This leads to a decrease in autophagic flux of amino acids causing a reduction in TORC1 and upregulation of autophagy. Supplementing the *trpml*$^{1}$ diet with protein-rich yeast reverses the effects of diminished TORC1 activity. These findings raise the possibility that patients with mucolipidosis type IV (MLIV) may also show diminished TORC1 activity. If so, it is intriguing to speculate that amino

(F) Model of TRPML function in regulating endosomal trafficking and TORC1 activity. PM, plasma membrane; EE, early-endosome; LE, late-endosome; aut, autophagosome; lys, lysosome.

See Figure S4.

acid supplementation might reduce the severity of the clinical manifestations associated with MLIV.

### Supplemental Information

Supplemental Information includes four figures and Supplemental Experimental Procedures and can be found with this article online at http://dx.doi.org/10.1016/j.cub.2012.06.055.

### Acknowledgments

We thank the Bloomington Stock Center for fly stocks and FlyBase for valuable genome information. We also thank Geoffrey Broadhead and Hongxiang Hu for technical assistance, the IBP Cytodynamic Imaging Facility, and Hugo Bellen for providing reagents. C.M. was supported by grants from the March of Dimes and the National Eye Institute (EY10852).

Received: August 31, 2011
Revised: April 13, 2012
Accepted: June 15, 2012
Published online: August 2, 2012

### References

1. Venkatachalam, K., Long, A.A., Elsaesser, R., Nikolaeva, D., Broadie, K., and Montell, C. (2008). Motor deficit in a *Drosophila* model of mucolipidosis type IV due to defective clearance of apoptotic cells. Cell *135*, 838–851.
2. Brand, A.H., and Perrimon, N. (1993). Targeted gene expression as a means of altering cell fates and generating dominant phenotypes. Development *118*, 401–415.
3. Venkatachalam, K., Hofmann, T., and Montell, C. (2006). Lysosomal localization of TRPML3 depends on TRPML2 and the mucolipidosis-associated protein TRPML1. J. Biol. Chem. *281*, 17517–17527.
4. Rusten, T.E., Rodahl, L.M., Pattni, K., Englund, C., Samakovlis, C., Dove, S., Brech, A., and Stenmark, H. (2006). Fab1 phosphatidylinositol 3-phosphate 5-kinase controls trafficking but not silencing of endocytosed receptors. Mol. Biol. Cell *17*, 3989–4001.
5. Dubois, L., Lecourtois, M., Alexandre, C., Hirst, E., and Vincent, J.P. (2001). Regulated endocytic routing modulates wingless signaling in *Drosophila* embryos. Cell *105*, 613–624.
6. Klionsky, D.J. (2007). Autophagy: from phenomenology to molecular understanding in less than a decade. Nat. Rev. Mol. Cell Biol. *8*, 931–937.
7. Rubinsztein, D.C. (2006). The roles of intracellular protein-degradation pathways in neurodegeneration. Nature *443*, 780–786.
8. Fader, C.M., and Colombo, M.I. (2009). Autophagy and multivesicular bodies: two closely related partners. Cell Death Differ. *16*, 70–78.
9. Metcalf, D., and Isaacs, A.M. (2010). The role of ESCRT proteins in fusion events involving lysosomes, endosomes and autophagosomes. Biochem. Soc. Trans. *38*, 1469–1473.
10. Pryor, P.R., Reimann, F., Gribble, F.M., and Luzio, J.P. (2006). Mucolipin-1 is a lysosomal membrane protein required for intracellular lactosylceramide traffic. Traffic *7*, 1388–1398.
11. Vergarajauregui, S., and Puertollano, R. (2006). Two di-leucine motifs regulate trafficking of mucolipin-1 to lysosomes. Traffic *7*, 337–353.
12. Thompson, E.G., Schaheen, L., Dang, H., and Fares, H. (2007). Lysosomal trafficking functions of mucolipin-1 in murine macrophages. BMC Cell Biol. *8*, 54.
13. Dong, X.P., Shen, D., Wang, X., Dawson, T., Li, X., Zhang, Q., Cheng, X., Zhang, Y., Weisman, L.S., Delling, M., and Xu, H. (2010). PI(3,5)P(2) controls membrane trafficking by direct activation of mucolipin $Ca^{2+}$ release channels in the endolysosome. Nat. Commun. *1*, 38.
14. Lindmo, K., Simonsen, A., Brech, A., Finley, K., Rusten, T.E., and Stenmark, H. (2006). A dual function for Deep orange in programmed autophagy in the *Drosophila melanogaster* fat body. Exp. Cell Res. *312*, 2018–2027.
15. Xu, H., Delling, M., Li, L., Dong, X., and Clapham, D.E. (2007). Activating mutation in a mucolipin transient receptor potential channel leads to melanocyte loss in varitint-waddler mice. Proc. Natl. Acad. Sci. USA *104*, 18321–18326.
16. Dong, X.P., Cheng, X., Mills, E., Delling, M., Wang, F., Kurz, T., and Xu, H. (2008). The type IV mucolipidosis-associated protein TRPML1 is an endolysosomal iron release channel. Nature *455*, 992–996.
17. Lloyd-Evans, E., Morgan, A.J., He, X., Smith, D.A., Elliot-Smith, E., Sillence, D.J., Churchill, G.C., Schuchman, E.H., Galione, A., and Platt, F.M. (2008). Niemann-Pick disease type C1 is a sphingosine storage disease that causes deregulation of lysosomal calcium. Nat. Med. *14*, 1247–1255.
18. Scott, R.C., Schuldiner, O., and Neufeld, T.P. (2004). Role and regulation of starvation-induced autophagy in the *Drosophila* fat body. Dev. Cell *7*, 167–178.
19. Rusten, T.E., Lindmo, K., Juhász, G., Sass, M., Seglen, P.O., Brech, A., and Stenmark, H. (2004). Programmed autophagy in the *Drosophila* fat body is induced by ecdysone through regulation of the PI3K pathway. Dev. Cell *7*, 179–192.
20. Komatsu, M., and Ichimura, Y. (2010). Selective autophagy regulates various cellular functions. Genes Cells *15*, 923–933.
21. Yu, L., McPhee, C.K., Zheng, L., Mardones, G.A., Rong, Y., Peng, J., Mi, N., Zhao, Y., Liu, Z., Wan, F., et al. (2010). Termination of autophagy and reformation of lysosomes regulated by mTOR. Nature *465*, 942–946.
22. Avruch, J., Long, X., Ortiz-Vega, S., Rapley, J., Papageorgiou, A., and Dai, N. (2009). Amino acid regulation of TOR complex 1. Am. J. Physiol. Endocrinol. Metab. *296*, E592–E602.
23. Chang, Y.Y., Juhász, G., Goraksha-Hicks, P., Arsham, A.M., Mallin, D.R., Muller, L.K., and Neufeld, T.P. (2009). Nutrient-dependent regulation of autophagy through the target of rapamycin pathway. Biochem. Soc. Trans. *37*, 232–236.
24. Zoncu, R., Efeyan, A., and Sabatini, D.M. (2011). mTOR: from growth signal integration to cancer, diabetes and ageing. Nat. Rev. Mol. Cell Biol. *12*, 21–35.
25. Asha, H., Nagy, I., Kovacs, G., Stetson, D., Ando, I., and Dearolf, C.R. (2003). Analysis of Ras-induced overproliferation in *Drosophila* hemocytes. Genetics *163*, 203–215.
26. Sevrioukov, E.A., He, J.P., Moghrabi, N., Sunio, A., and Krämer, H. (1999). A role for the deep orange and carnation eye color genes in lysosomal delivery in *Drosophila*. Mol. Cell *4*, 479–486.
27. Kim, E., Goraksha-Hicks, P., Li, L., Neufeld, T.P., and Guan, K.L. (2008). Regulation of TORC1 by Rag GTPases in nutrient response. Nat. Cell Biol. *10*, 935–945.
28. Stocker, H., Radimerski, T., Schindelholz, B., Wittwer, F., Belawat, P., Daram, P., Breuer, S., Thomas, G., and Hafen, E. (2003). Rheb is an essential regulator of S6K in controlling cell growth in *Drosophila*. Nat. Cell Biol. *5*, 559–565.
29. Zhang, H., Stallock, J.P., Ng, J.C., Reinhard, C., and Neufeld, T.P. (2000). Regulation of cellular growth by the *Drosophila* target of rapamycin dTOR. Genes Dev. *14*, 2712–2724.
30. Pryor, P.R., Mullock, B.M., Bright, N.A., Gray, S.R., and Luzio, J.P. (2000). The role of intraorganellar Ca(2+) in late endosome-lysosome heterotypic fusion and in the reformation of lysosomes from hybrid organelles. J. Cell Biol. *149*, 1053–1062.
31. Bernal, A., and Kimbrell, D.A. (2000). *Drosophila* Thor participates in host immune defense and connects a translational regulator with innate immunity. Proc. Natl. Acad. Sci. USA *97*, 6019–6024.
32. Miron, M., Verdú, J., Lachance, P.E., Birnbaum, M.J., Lasko, P.F., and Sonenberg, N. (2001). The translational inhibitor 4E-BP is an effector of PI(3)K/Akt signalling and cell growth in *Drosophila*. Nat. Cell Biol. *3*, 596–601.
33. Lee, C.Y., and Baehrecke, E.H. (2001). Steroid regulation of autophagic programmed cell death during development. Development *128*, 1443–1455.
34. Hennig, K.M., Colombani, J., and Neufeld, T.P. (2006). TOR coordinates bulk and targeted endocytosis in the *Drosophila melanogaster* fat body to regulate cell growth. J. Cell Biol. *173*, 963–974.
35. MacGurn, J.A., Hsu, P.C., Smolka, M.B., and Emr, S.D. (2011). TORC1 regulates endocytosis via Npr1-mediated phosphoinhibition of a ubiquitin ligase adaptor. Cell *147*, 1104–1117.

**Current Biology, Volume *22***

## Supplemental Information

# *Drosophila* TRPML Is Required for TORC1 Activation

**Ching-On Wong, Ruoxia Li, Craig Montell, and Kartik Venkatachalam**

### Supplemental Inventory

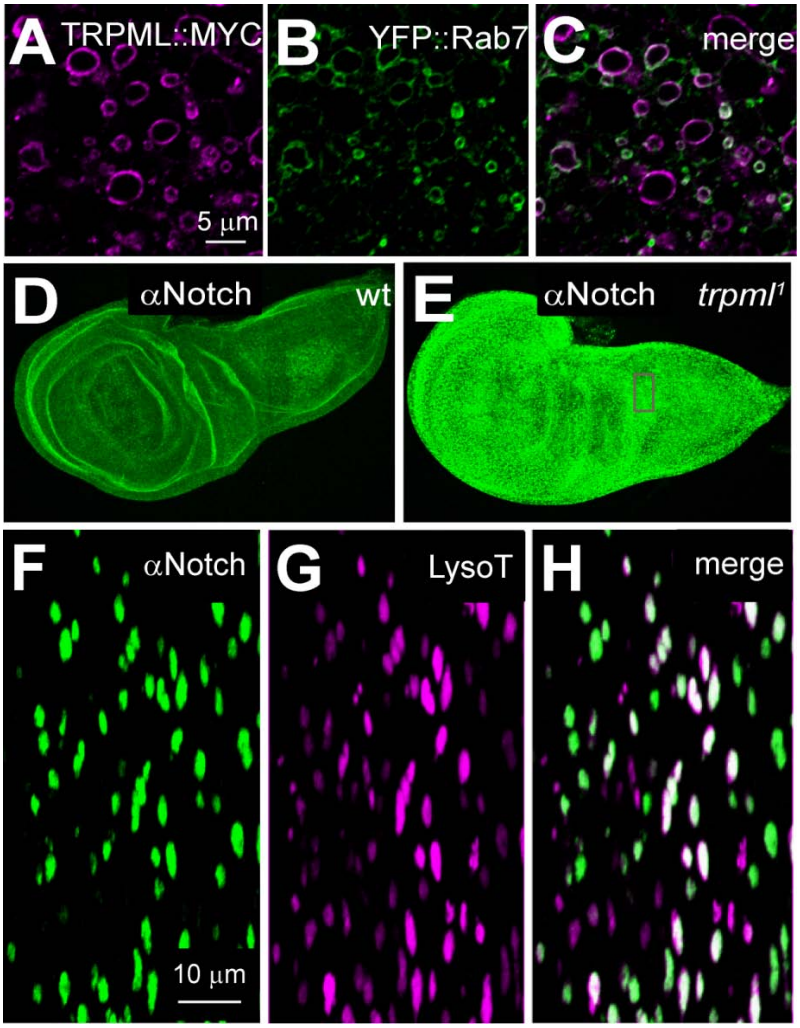


**Figure S1.**
(A-C) TRPML::MYC (A, magenta) colocalizes with YFP::Rab7-positive vesicles (B, green) *in vivo*. Confocal images of 3rd instar larval fat bodies dissected from animals expressing *UAS-trpml::myc* under the control of fat-body specific *cg-GAL4*. The TRPML::MYC localization was detected using anti-MYC.
(C) Merged image of (A-B). Scale bar shown in (A) applies to (A-C).
(D-E) Wild-type (wt) (D) and *trpml*$^{1}$. (E) 3rd instar larval (96 hours old) wing discs stained with anti-Notch (Notch).
(F-H) Magnified images of the boxed area from (E) showing partial co-localization of Notch (F) with LysoTracker-positive vesicles (G) in the *trpml*$^{1}$ mutant wing discs. The scale bar shown in (F) applies to (F-H).

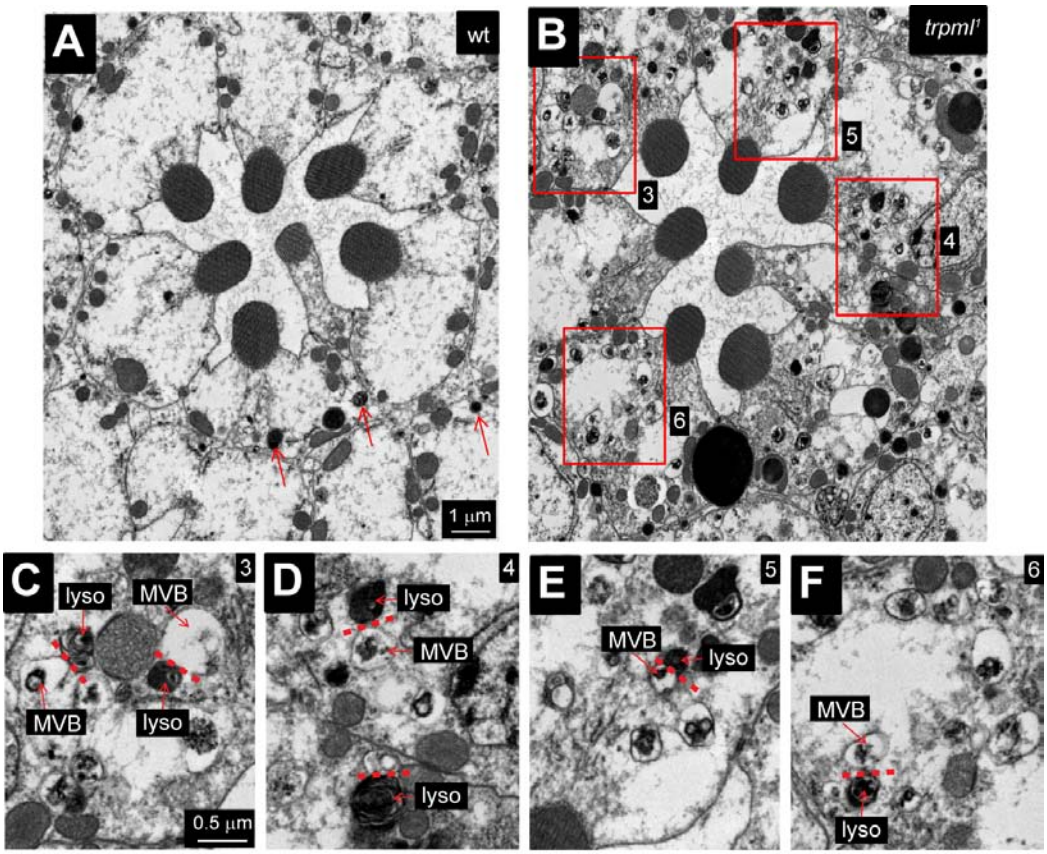


**G**

| organelles per ommatidia | wt | *trpml*$^{1}$ | (p<0.05) |
|---|---|---|---|
| MVBs | 1.4 ±1.2 | 16.4 ±2.3 | yes |
| lysosomes | 0.5 ±0.2 | 4.7 ±1.1 | yes |
| fusion primed vesicles | 0.1 ±0.1 | 2.2 ±0.8 | yes |
| autophagosomes | 1.3 ±0.4 | 1.9 ±0.3 | yes |
| autolysosomes | 1.2 ±0.2 | 1.4 ±1.1 | no |

**Figure S2.**
(A-B) Representative transmission EM images of 1-2 week old adult photoreceptor cells from wild-type (wt) (A) and *trpml*$^{1}$ (B) animals. The red arrows indicate electron dense lysosomes. This analysis focused on photoreceptor cell bodies because we demonstrated previously that they show defects in autophagy, and these cells are particularly amenable to ultrastructural analyses. Scale bar shown in (A) also applies to (B).
(C) Box 3 from (B).
(D) Box 4 from (B).
(E) Box 5 from (B).
(F) Box 6 from (B).
The scale bar shown in (C) also applies to (D-F).
The structures labeled include lysosomes (lyso) and multivesicular bodies (MVB). The dashed red lines indicate the area of contact between the “fusion-clamped” vesicles.
(G) Quantification of the number of indicated vesicles per ommatidium. Values represent mean ±SEM. Significance was determined using the Student’s t-test. Numbers of wt and *trpml*$^{1}$ animals analyzed were 5 and 8 respectively. ≥5 randomly chosen ommatidia were analyzed from each animal.

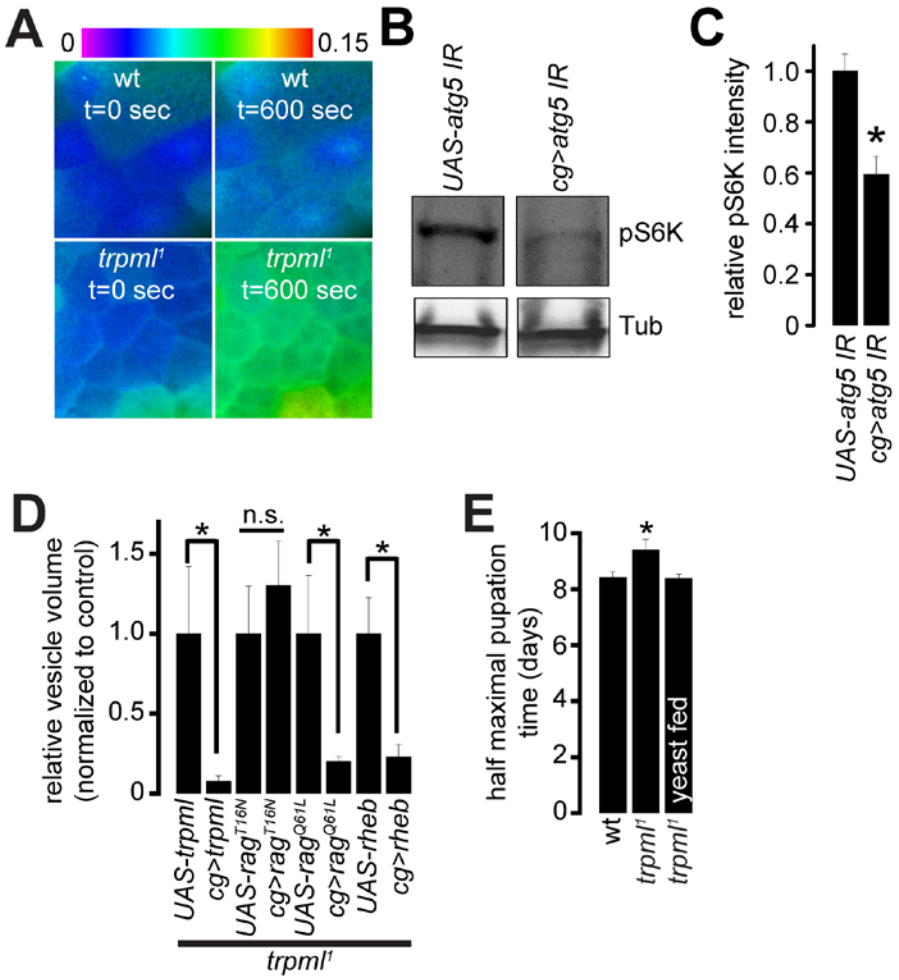


**Figure S3.**

(A) Representative pseudocolored images showing changes in the Fura-2 $F_{340}/F_{380}$ ratio in wild-type (wt) and *trpml*$^{1}$ fat-bodies following treatment with 500 nM bafilomycin A1. Images from the beginning (t=0 sec), and end of the experiment (t=600 sec) are shown. Scale bar shows the relationship between the psuedocolor and $F_{340}/F_{380}$ ratio.

(B) Representative Western blot of larval fat-body extracts derived from control (*UAS-atg5 IR*) and *cg>atg5 IR* 3$^{rd}$ instar larvae probed with antibodies against phosphorylated S6K (pS6K) and α-tubulin (tubulin).

(C) Quantification of relative pS6K intensities in fat-body extracts derived from wandering 3$^{rd}$ instar larvae of the indicated genotypes and feeding status. Values were normalized to wt. Values represent mean ±SEM. "*" indicates $p<0.05$, Student's t-test (n=5 independent samples of each genotype). The term *cg* refers to *cg-GAL4*, which is a fat-body and hemocyte specific driver.

(D) Bar graph showing the relative volumes of LysoTracker-positive vesicles in fat-bodies dissected from 3$^{rd}$ instar *trpml*$^{1}$ larvae expressing the indicated transgenes. Values were normalized to the *UAS* control for each experimental pair. Values represent mean ±SEM. "*" represents $p<0.05$, Student's t-test (n=5-9 animals per genotype).

(E) Bar graph showing the half maximal pupation times for wt, *trpml*$^{1}$, and *trpml*$^{1}$ reared on a diet containing additional 20% (w/v) yeast. Values represent mean ±SEM. "*" indicates $p<0.05$, ANOVA (n≥3 independent fly vials).

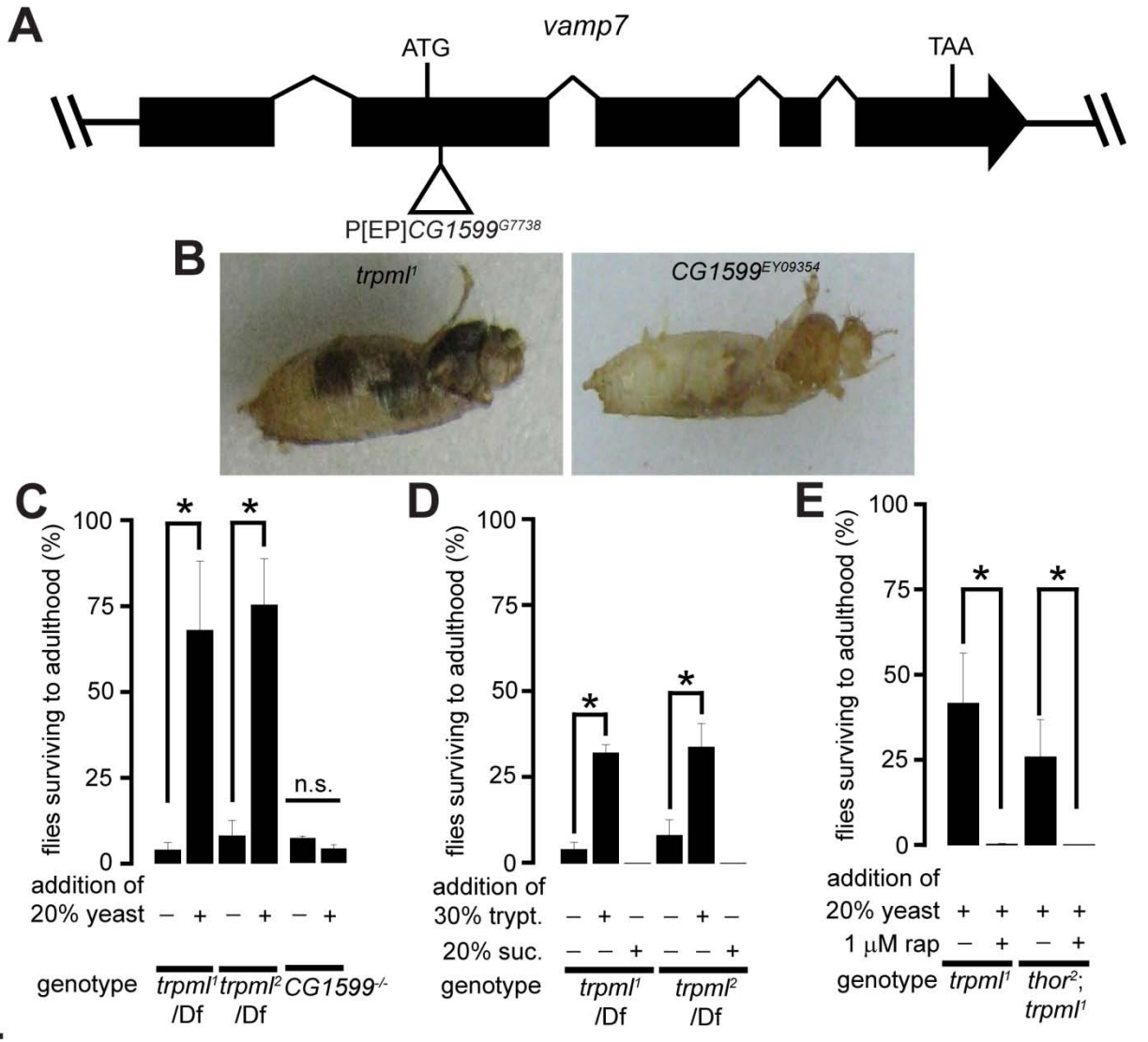
A
vamp7
ATG
TAA
P[EP]CG1599G7738
B
trpml1
CG1599EY09354
C
flies surviving to adulthood (%)
100
75
50
25
0
*
*
n.s.
addition of
20% yeast – + – + – +
genotype
trpml1 /Df
trpml2 /Df
CG1599-/-
D
flies surviving to adulthood (%)
100
75
50
25
0
*
*
addition of
30% trypt. – + – – + –
20% suc. – – + – – +
genotype
trpml1 /Df
trpml2 /Df
E
flies surviving to adulthood (%)
100
75
50
25
0
*
*
addition of
20% yeast + + + +
1 μM rap – + – +
genotype
trpml1
thor2; trpml1
F
TRPML::MYC
LysoT
merge
sg
fb

**Figure S4.**
(A) The *vamp7* (*CG1599*) genomic locus. The open triangle shows the P-element insertion site within the coding sequence. (B) Representative images of flies of the indicated genotypes that died following partial eclosion from the pupal cases.
(C) Bar graph showing survival of flies of the indicated genotypes that were reared on either standard food or food containing 20% yeast. Values represent mean ±SEM. "*" indicates $p<0.05$, Student's t-test ($n\geq3$ independent fly vials); n.s. indicated no significance.
(D) Bar graph showing survival of flies of the indicated genotypes that were reared on either standard food or food containing the indicated additional feedants: trypt. (tryptone) or suc. (sucrose). Values represent means ±SEM. "*" indicates $p<0.05$, ANOVA followed by pairwise Student's t-test with Bonferroni post-hoc corrections ($n\geq3$ independent fly vials).
(E) Survival of flies of the indicated genotypes that were reared on standard cornmeal and molasses food containing the indicated additions: 20% yeast paste and 1 μM rapamycin (rap). Values represent mean ±SEM. "*" indicates $p<0.05$, Student's t-test ($n\geq3$ independent fly vials).
(F) Representative confocal images showing TRPML::MYC and LysoTracker staining in 3$^{rd}$ instar salivary glands (sg) and fat-bodies (fb, demarcated by the white dashed lines). Note that although TRPML::MYC decorates the periphery of the LysoTracker-positive vesicles in the fat-bodies, it is localized at the cell cortex in the salivary gland, an organ with very low levels of autophagy (consistent with no LysoTracker staining) during this developmental stage.

## Supplemental Experimental Procedures

### Generation of *UAS-trpml::myc* Transgenic Flies

We generated the *UAS-trpml::myc* flies by fusing the DNA sequence encoding the c-myc epitope (EQKLISEEDL) to the 3' end of the *trpml* cDNA. We subcloned the *trpml::myc* cDNA into the pUAST vector and obtained transgenic flies (generated by BestGene Inc.).

### Fly Stocks and Husbandry

The existing fly lines used in this study were *UAS-YFP::Rab7* (Bloomington line 23270), *UAS-LAMP::GFP* [1], *UAS-GFP::ATG8* [2], $trpml^{1}$ and $trpml^{2}$ [3], *cg-GAL4* (Bloomington line 7011), *lsp2-GAL4* (Bloomington line 6357), P[$trpml^{+}$] [3], *UAS-trpml* [3], $dor^{4}$ (Bloomington line 35), $dor^{1}$ (Bloomington line 751) $dor^{8}$ (Bloomington line 28), *UAS-*$rag^{Q61L}$ and *UAS-*$rag^{T16N}$ [4], *UAS-rheb* (Bloomington line 28488), $CG1599^{EY09354}$ (Bloomington line 28488), $thor^{2}$ (Bloomington line 9559), and the deficiency uncovering *trpml*, Df(3L)Exel6135 (Bloomington line 7614). All flies were reared at room temperature (~22°C).

The ingredients in 1 L of liquid fly food were: 95 g agar, 275 g Brewer's yeast, 520 g of cornmeal, 110 g of sugar, and 45 g of propionic acid. 36 g of Tegosept was dissolved in 92 ml of 95% ethanol and added to the mixture to prevent bacterial growth.

### Feeding Experiments

Crosses were set up with 20-30 adult flies in 25-mm vials containing the above-mentioned fly food. After 7-days of egg-laying, the $F_0$ flies were cleared and solutions of 20% yeast, 30% tryptone or 20% sucrose (1-1.5 ml) were laid on top of the food. For the rapamycin treatment experiments, 5 g of instant fly food (formula 4-24 plain, Carolina Biological Supply Company) with or without an additional 1 g of yeast was suspended in water with or without rapamycin (1 µM final concentration). Subsequently, crosses were set up with 20-30 adult flies. After 7-days, the $F_0$ flies were cleared, and vials were watered every 2-3 days to keep the food moist.

### Immunohistochemistry, Confocal Microscopy and Image Analysis

LysoTracker and antibody staining were performed on larval tissues dissected from 3$^{rd}$ instar wandering larvae. Larvae were pinned and immobilized on cured Sylgard silicone elastomer (Dow Corning), and bathed in ice-cold HL-3 saline (70 mM NaCl, 5 mM KCl, 20 mM $MgCl_2$, 10 mM $NaHCO_3$, 0.5 mM $CaCl_2$, 115 mM sucrose, 5 mM trehalose, and 5 mM HEPES; pH 7.2.). Fat bodies and wing-discs were dissected from the pinned larvae and incubated in HL-3 containing LysoTracker Red DND-99 (1:500) (Invitrogen) at room temperature for 45 minutes. The samples were then washed 3-times with HL-3, and fixed in 4% paraformaldehyde in phosphate buffered saline (PBS) for 20 minutes. When LysoTracker staining was not performed, larval tissues were fixed immediately after dissection. Samples were then washed 3 times with PBS plus 0.1% Triton X-100 before incubating with the primary antibodies. The following primary antibodies were used in the experiments: 4D4 mouse anti-Wg (1:100), 1G9 mouse Hnt (1:40), C458.2H mouse Notch (1:40), rabbit anti-GFP (1:250) (Invitrogen), and mouse anti-c-Myc (1:500) (Sigma). The Wg, Hnt and Notch monoclonal antibodies were obtained from the Developmental Studies Hybridoma Bank developed under the auspices of the NICHD and maintained by The University of Iowa, Department of Biology, Iowa City, IA 52242. After incubation with the primary antibodies overnight at 4$^{o}$C, the tissue were washed and probed with fluorophore-conjugated secondary antibodies (Alexa Fluor 488/568 goat anti-mouse) (Invitrogen) at room temperature for 1.5 hours. Samples were mounted on glass slide with Vectashield Mounting Media containing DAPI (Vector Labs).

Confocal images were recorded using a Nikon A1 Confocal Laser Microscope System (Nikon), and analyzed using Image-Pro Plus (Media Cybernetics). For 3-dimensional reconstructions, Z-series were exported as TIFF files into the Image-Pro Plus software. 3-dimensional reconstructions were made using the following parameters: 2x2x1 subsampling, 3x3x3 lo-pass filter, and a surface value of 125.

**Transmission EM**

Fat bodies or wing-discs were dissected from wandering third-instar larvae, and fixed with 4% paraformaldehyde and 0.2% glutaraldehyde in 0.1 M sodium phosphate buffer (pH 7.4) at 4 °C for at least 2 hours. Samples were then washed, and stained with 0.5% osmium tetroxide on ice for 1 hour. After a series of washing, dehydrating with ethanol and serial infiltration with LR white resin (#14381, Electronic Microscopy), the samples were then individually embedded in 100% resin held by gelatinous capsules. Curing was done at approximately 55 degree Celsius for 2 days.

For immuno-EM, fat bodies were collected and fixed as described above. All the procedures were done at 4 degree Celsius except embedding. After fixation, the samples were incubated successively with 0.12% tannic acid, 50 mM $NH_4Cl$, and 2% uranyl acetate for 30 minutes in each step. Dehydration, resin infiltration and embedding were done as described above.

**Western Blots**

Fat bodies dissected from 3$^{rd}$ instar larvae were boiled in 2x Laemmli Sample Buffer (Bio-Rad) and 20% β-mercaptoethanol for 15 minutes. Supernatants from the centrifuged samples were loaded onto 10% Tris-glycine polyacrylamide gels (BioRad) for SDS-PAGE. Fractionated proteins were transferred to nitrocellulose membranes (GE Healthcare) in Tris-glycine buffer. The blots were probed with mouse anti-tubulin (1:1000) (Developmental Studies Hybridoma Bank, Iowa University), and rabbit anti-pS6K (1:1000) (#9209S, Cell Signaling Technology). After overnight incubations with the primary antibodies, the blots were washed and probed with IRDye 680 donkey anti-rabbit IgG (LI-COR) and IRDye 800 donkey anti-mouse IgG (LI-COR), and signals were detected with the Odyssey infrared imaging system (LI-COR). Blot images were analyzed using ImageJ (National Institute of Health).

**Pupation Timing**

Crosses were set up with 20-30 adult flies in 25-mm vials with standard corn meal and sugar food (containing 2.75% w/v yeast) at room temperature (~22$^{o}$C). After 24 hours of egg deposition, parental adults were removed from the vials. All vials were maintained at room temperature and watered every 2-3 days to keep the food moist. In the yeast-fed experimental group, 40% (w/v) yeast paste (0.5-1 ml) was laid on the top of the food on day 5. The numbers of pupal cases on the walls of the vials were recorded daily.

**Subcellular Localization of TRPML in Figure 4**

5g of instant fly food (formula 4-24 plain, Carolina Biological Supply Company) with an additional 1g of yeast was suspended in water with or without rapamycin (1 μM final concentration) in 25-mm vials. Crosses set up with 20-30 adult flies were allowed to lay eggs for 24 hours. On day 5, 40% (w/v) yeast paste (0.5-1 ml) with or without 1 μM rapamycin was laid on the top of the food. Fat bodies from wandering 3$^{rd}$-instar larvae were dissected and fixed. Immunohistochemistry and imaging were done as described above.

## Fat-body Calcium Imaging

Fat bodies were dissected from wandering 3$^{rd}$-instar larva in HL-3 saline, and transferred to Schneider's insect medium (Sigma) containing 20 µM Fura-2/AM (Invitrogen) and 100 nM probenecid (Sigma) for 1 hour at room temperature. The tissues were then washed briefly and bathed in Schneider's insect medium with 100 nM probenecid. Tissue loaded with Fura-2 was gently pressed to the bottom of a poly-D-lysine (MP Biomedicals) coated glass bottom culture dish (MatTek) with 200 µL of HL-3 saline containing 2 mM $CaCl_2$. Fluorescence images were acquired by 340/380 nm excitation and 510 nm emission, using Nikon TiE Wide-Field Fluorescence Imaging System (Nikon). The background subtracted $Ca^{2+}$ ratio ($R_{340/380}$) was measured and calculated by NIS Elements imaging software (Nikon). Bafilomycin A1 (Sigma) stock solution was prepared at 500 µM in DMSO. After base-line fluorescence images were acquired for at least 1 minute, approximately 50 µL of bath solution was pipetted out to dilute bafilomycin A1 and added back to the bath at a final concentration of 500 nM.

## Thapsigargin Treatment

3$^{rd}$-instar larval fat bodies were dissected in HL-3 saline (0.5 mM $CaCl_2$) and LysoTracker Red DND-99 (1:500). After 15-minute incubation at room temperature, 5 µM thapsigargin or equivalent volume of DMSO (vehicle control) was added to the bath for 15-minutes. The tissues were then immediately washed once in plain HL-3 saline and fixed with 4% paraformaldehyde. Sample mounting and imaging were done as described above.

## Supplemental References


1. Pulipparacharuvil, S., Akbar, M.A., Ray, S., Sevrioukov, E.A., Haberman, A.S., Rohrer, J., and Krämer, H. (2005). *Drosophila* Vps16A is required for trafficking to lysosomes and biogenesis of pigment granules. J. Cell Sci. *118*, 3663-3673.
2. Rusten, T.E., Vaccari, T., Lindmo, K., Rodahl, L.M., Nezis, I.P., Sem-Jacobsen, C., Wendler, F., Vincent, J.P., Brech, A., Bilder, D., et al. (2007). ESCRTs and Fab1 regulate distinct steps of autophagy. Curr. Biol. *17*, 1817-1825.
3. Venkatachalam, K., Long, A.A., Elsaesser, R., Nikolaeva, D., Broadie, K., and Montell, C. (2008). Motor deficit in a *Drosophila* model of mucolipidosis type IV due to defective clearance of apoptotic cells. Cell *135*, 838-851.
4. Kim, E., Goraksha-Hicks, P., Li, L., Neufeld, T.P., and Guan, K.L. (2008). Regulation of TORC1 by Rag GTPases in nutrient response. Nat. Cell Biol. *10*, 935-945.